Band twisting and resilience to disorder in long-range topological superconductors

Citation: Puel, T. O. and O. Viyuela. "Band twisting and resilience to disorder in long-range topological superconductors." Physical Review B 100, 1 (July 2019): 014508 (2019) © 2019 American Physical Society

As Published: http://dx.doi.org/10.1103/PhysRevB.100.014508

Publisher: American Physical Society

Persistent URL: https://hdl.handle.net/1721.1/136946

Version: Final published version: final published article, as it appeared in a journal, conference proceedings, or other formally published context

Band twisting and resilience to disorder in long-range topological superconductors

T. O. Puel*
Beijing Computational Science Research Center, Beijing 100193, China;
CeFEMA, Instituto Superior Técnico, Universidade de Lisboa, Avenida Rovisco Pais, 1049-001 Lisboa, Portugal;
and Zhejiang Institute of Modern Physics, Zhejiang University, Hangzhou, Zhejiang 310027, China

O. Viyuela†
Department of Physics, Harvard University, Cambridge, Massachusetts 02318, USA
and Department of Physics, Massachusetts Institute of Technology, Cambridge, Massachusetts 02139, USA

(Received 22 March 2019; revised manuscript received 27 June 2019; published 11 July 2019)

Planar topological superconductors with power-law-decaying pairing display different kinds of topological phase transitions where quasiparticles dubbed nonlocal-massive Dirac fermions emerge. These exotic particles form through long-range interactions between distant Majorana modes at the boundary of the system. We show how these propagating-massive Dirac fermions neither mix with bulk states nor Anderson-localize up to large amounts of static disorder despite having finite energy. Analyzing the density of states (DOS) and the band spectrum of the long-range topological superconductor, we identify the formation of an edge gap and a surprising double-peak structure in the DOS which can be linked to a twisting of energy bands with nontrivial topology. Our findings are amenable to experimental verification in the near-future using atom arrays on conventional superconductors, planar Josephson junctions on two-dimensional electron gases, and Floquet driving of topological superconductors.

DOI: 10.1103/PhysRevB.100.014508

I. INTRODUCTION

Symmetry-protected topological orders are quantum phases of matter characterized by nonlocal order parameters (topological invariants) and protected edge states at the boundary [1,2]. Symmetry-protected topological phases with particle-hole symmetry give rise to topological superconductors [3,4] with unconventional pairing and gapless edge states, dubbed Majorana zero modes. Majorana zero modes are nonabelian anions, which can be braided to perform topological quantum computation and are protected against thermal fluctuations by a superconducting gap [5–9]. These unpaired Majorana particles were first shown to arise at the ends of a chain of fermions with p-wave superconducting pairing [10]. However, the impracticality of p-wave pairing in nature was initially believed to be a roadblock, until proximity-induced superconductivity schemes proved to be a way to circumvent this obstacle [11].

In recent years, different experiments have shown Majorana physics by means of a conventional superconductor proximitized to the surface of a topological insulator [11–13], semconductor nanowires with strong spin-orbit coupling and subject to Zeeman fields [13–29], quantum anomalous Hall insulator-superconductor structures [28], and atomic arrays on superconducting substrates [30–46]. In particular, one-dimensional (1D) arrays of magnetic impurities [41,47], where the length of the chain is relatively small compared to the coherence length of the host superconductor [30], generate an effective p-wave Hamiltonian with long-range pairing [30,32–37]. Floquet driving of a p-wave superconductor [48] and planar Josephson junctions proximitized to a 2D electron gas with spin-orbit coupling and Zeeman field [49–51] also give rise to effective models of topological superconductivity with long-range couplings.

Inspired by these recent experimental developments, p-wave Hamiltonians with long-range couplings have been thoroughly studied [52–68]. A long-range extension of the Kitaev chain with power-law-decaying hopping and pairing amplitudes gives rise to a combined exponential and algebraic decay of correlations, breakdown of conformal symmetry, and violation of the area law of entropy [54,56]. The topological nature of this new model has also been unveiled [57], demonstrating the existence of fractional topological numbers associated with nonlocal-massive Dirac fermions [57,61,62]. These particles are fermions with a highly nonlocal extension, as they are formed out of the long-range interaction of distant Majorana particles at the edge, and their localization properties are indeed robust to weak static disorder [57]. Interestingly, a staircase of higher-order topological phase transitions can be induced by tuning the exponent of the power-law-decaying pairing amplitude [65].

Generalizations of the long-range Kitaev chain to two dimensions have been constructed [67,68], where the p-wave character of the superconductor is preserved while including power-law-decaying couplings that extend over the plane. In these systems, topological phases holding propagating Majorana edge states with different chiralities are significantly enhanced by long-range couplings. In one of the topological

*tharnier@csrc.ac.cn
†oviyuela@fas.harvard.edu

phases, propagating Majorana fermions at each edge pair nonlocally and become gapped for sufficiently long-range interactions, while remaining topological and localized at the boundary [67]. However, the robustness of these new chiral edge states with respect to general static disorder was unclear and the effects of the long-range couplings in the band spectrum of the topological superconductor were not explored.

In this article, we study how propagating Majorana states, which become gapped by the effect of long-range interactions, are affected by the inclusion of static disorder. We show how the localization at the edge is preserved even for very strong disorder, demonstrating that the propagating massive Dirac fermions at the edge are not pushed to the bulk or delocalized. This is one of the characteristic features of all topologically protected edge states. Moreover, we study how the band spectrum of a planar p-wave topological superconductor is modified by the effect of long-range couplings. We prove how a characteristic (and previously unnoticed) double-peak structure in the density of states (DOS) of the topological superconductor is enhanced by the inclusion of power-law-decaying amplitudes. Associated with this effect we find a band twisting in the energy spectrum provided the phase is topologically nontrivial.

The paper is structured as follows. In Sec. II, we introduce the 2D p-wave Hamiltonian with long-range couplings and perform a detailed study of the band structure and the density of states as a function of the decay exponents. In Sec. III we demonstrate the robustness of the nonlocal-massive Dirac fermions due to disorder and compare it to the case with unpaired Majoranas through the spatial distribution of these nonlocal-massive Dirac fermions. Section IV is devoted to conclusions. In Appendix A we perform a finite-size scaling of in-gap states and their dependence on the decay exponent α, and in Appendix B we analyze the robustness of the system with respect to different types of static disorder.

II. BAND STRUCTURE AND DENSITY OF STATES

The model studied in this paper is that of a two-dimensional spinless p-wave superconductor with long-range hopping and long-range superconducting coupling. In real space the Hamiltonian can be written as

$$H = -(\mu - 4t)\sum_{\boldsymbol{r}=1}^{N}(c_{\boldsymbol{r}}^{\dagger}c_{\boldsymbol{r}} - c_{\boldsymbol{r}}c_{\boldsymbol{r}}^{\dagger}) - \sum_{\boldsymbol{r}}\sum_{\boldsymbol{r}'\neq\boldsymbol{r}}\frac{t}{R^{\beta}}(c_{\boldsymbol{r}'}^{\dagger}c_{\boldsymbol{r}} + c_{\boldsymbol{r}}^{\dagger}c_{\boldsymbol{r}'}) - \sum_{\boldsymbol{r}}\sum_{\boldsymbol{r}'\neq\boldsymbol{r}}\frac{\Delta}{R^{\alpha+1}}[(R_x + iR_y)c_{\boldsymbol{r}'}^{\dagger}c_{\boldsymbol{r}}^{\dagger} + (R_x - iR_y)c_{\boldsymbol{r}}c_{\boldsymbol{r}'}], \tag{1}$$

where both $\boldsymbol{r}$ and $\boldsymbol{r}'$ run over all sites of a square lattice labeled from 1 to N, where N is the total number of sites. We have defined $\boldsymbol{R} = (R_x, R_y) \equiv \boldsymbol{r} - \boldsymbol{r}'$ and $|\boldsymbol{R}| = \sqrt{R_x^2 + R_y^2} \equiv R$. The band width is represented by t and the coupling strength is represented by Δ. The exponents α and β control the decay of the superconducting coupling range and hopping range, respectively. The chemical potential μ eventually drives the system to phase transitions; for example, in the regime of fast decay (large values of the decaying exponents) we find a transition from a trivial superconducting phase (SC) to a topological superconducting phase characterized by Majorana fermions ($\mathcal{M}$). Interestingly, it is known that long-range superconducting couplings give rise to new topological phases characterized by massive Dirac fermions ($\mathcal{D}$). This phase transition happens at the critical value $\alpha = 2$ and only exists for one of the two topological phases [67]. This differs from the semi-2D Hamiltonian [68], where the long-range terms appear only in the x and y directions. The phase transition then occurs at $\alpha = 1$ and is present in both topological phases. A phase diagram illustrating the former case is depicted in Fig. 1(a). Unless explicitly mentioned, we have used $t = 0.5$ as reference parameter, $\Delta = 0.5$ following Ref. [67], and $\beta = 10$, i.e., fast-decay hopping. For instance, we have verified that whatever β, $\alpha \geqslant 20$ gives the same energy spectrum of the pure short-range hopping, with next-nearest-neighbor hopping.

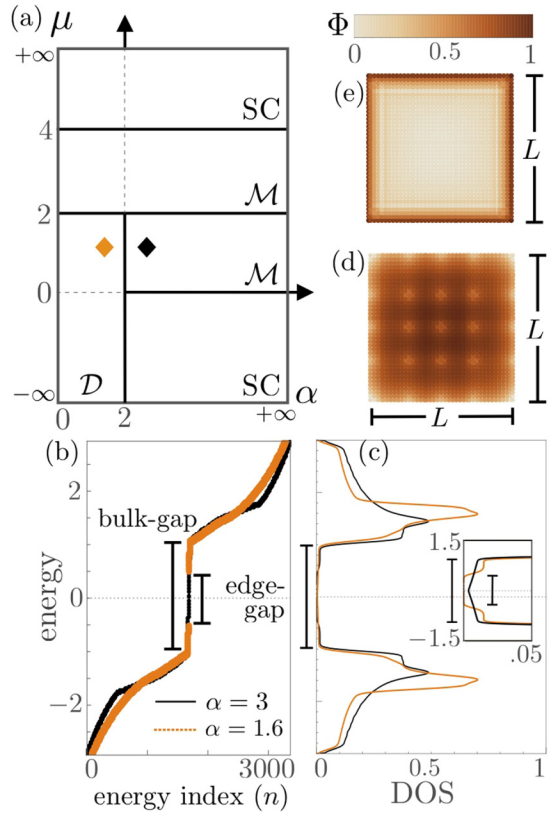

FIG. 1. (a) Phase diagram for a range of chemical potential, μ, and long-range superconducting coupling, α, parameters. Three phases can be identified: (i) a trivial superconducting phase, SC; (ii) a topological superconducting phase with Majorana fermions, $\mathcal{M}$; and (iii) a topological superconducting phase with massive Dirac fermions, $\mathcal{D}$. We note that the two different phases $\mathcal{M}$ have opposite chiralities. (b), (c) Energy spectrum and DOS, respectively, for the two topological phases (labeled in the phase diagram, using the same color code) in a system of size $N = 1681$. (d), (e) Probability of occupancy associated with the nth energy of the 2D finite-squared system (top view) in the $\mathcal{D}$ phase, as described in the previous panels. In particular, a representative probability of occupancy for a bulk energy is plotted in (d), while the lowest finite energy inside the gap is plotted in (e). Note that the probability of occupancy is plotted on log scale, thus written in terms of Φ as defined in the text.

A. Massive Dirac fermions

The first step is to identify the differences and similarities between the Majorana phase and the massive Dirac phase. For this, the edge-state excitations are analyzed.

By exact diagonalization $H|\psi_n\rangle = E_n|\psi_n\rangle$ we obtained the Bogoliubov energy spectrum, E_n with $n = 1, \ldots, 2N$, of a finite (squared) system with $L^2 \equiv N$ lattice sites. The results are depicted in Fig. 1, in which we exemplify the two topological phases $\mathcal{M}$ and $\mathcal{D}$. The parameters are indicated in the phase diagram [Fig. 1(a)] by the diamonds, namely, we set $\alpha = 1.6$ and $\alpha = 3$, with $\mu = 1$. In both phases, the superconducting gap (termed here the bulk gap) is easily noted from either the energy spectrum in Fig. 1(b) or its respective DOS in Fig. 1(c). The topological properties are manifested as in-gap states; in particular, the inset in Fig. 1(c) details the difference between the two topological phases [69]. While the Majorana states manifest as a finite DOS over the entire gap, the massive Dirac states let open a smaller gap (termed here the edge gap since it is the energy difference between edge-state excitations).

One may also look at the localization of massive Dirac states plotting the probability of occupancy related to the nth wave vector (corresponding to energy E_n inside the bulk gap) at each site, i.e., $\mathcal{P}_n(\boldsymbol{r}) \equiv a_n(\boldsymbol{r})a_n^*(\boldsymbol{r})$, where the amplitude $a_n(\boldsymbol{r})$ is obtained from $|\psi_n\rangle = \sum_{\boldsymbol{r}} a_n(\boldsymbol{r})|\psi_n(\boldsymbol{r})\rangle$, and the normalization implies $\sum_{\boldsymbol{r}} \mathcal{P}_n(\boldsymbol{r}) = 1$. Figures 1(d) and 1(e) exemplify this probability for an energy inside the bulk and for the lowest finite energy inside the bulk gap, respectively. The probability amplitude of occupancy is better analyzed if log scaled, thus for convenience we have defined a normalized logarithmic localization, $\Phi \equiv 1 - \log \mathcal{P}_n(\boldsymbol{r})/\log \mathcal{P}_{\min}$, where $\Phi = 1$ if $\mathcal{P}_n(\boldsymbol{r}) = 1$ and $\Phi = 0$ if $\mathcal{P}_n(\boldsymbol{r}) = \mathcal{P}_{\min}$. $\mathcal{P}_{\min}$ is the global-minimum probability $\mathcal{P}_n(\boldsymbol{r})$, i.e., among all energies E_n and all sites $\boldsymbol{r}$.

Equivalent to the Majorana excitations in the planar topological superconductor, the massive Dirac states are confined to the edges [see Fig. 1(e)], which form propagating modes protected by particle-hole symmetry. Technically speaking, the system still belongs to class D of topological superconductors [70] with a $\mathbb{Z}$ topological invariant [71]. In Fig. 1(d) we see the bulk energy excitations remaining spread over the sample. A thorough study of the robustness of the massive Dirac states is one of the main goals of this work and is discussed in Sec. III.

B. Twisted bands and double-peak structure

We discovered that the band spectrum and the DOS of our long-range topological superconductor provide valuable information regarding the energy distribution of the different eigenstates [see Fig. 1(c)]. In addition, we may extract useful quantities such as the magnitude of the superconducting gap, the group velocity, and the band dispersion.

For convenience, we consider a semi-infinite system, finite in the x direction and periodic in the y direction. As an example, let us take two points in the phases $\mathcal{M}$ in the phase diagram with different chiral edge states, namely, $\mu = 1$ and $\mu = 3$, with $\alpha = 3$. Figure 2(a) shows the DOS of these two points, while Figs. 2(b) and 2(c) show their respective band spectra for a semi-infinite system. From these figures we highlight the following: (i) associated with the peak structures

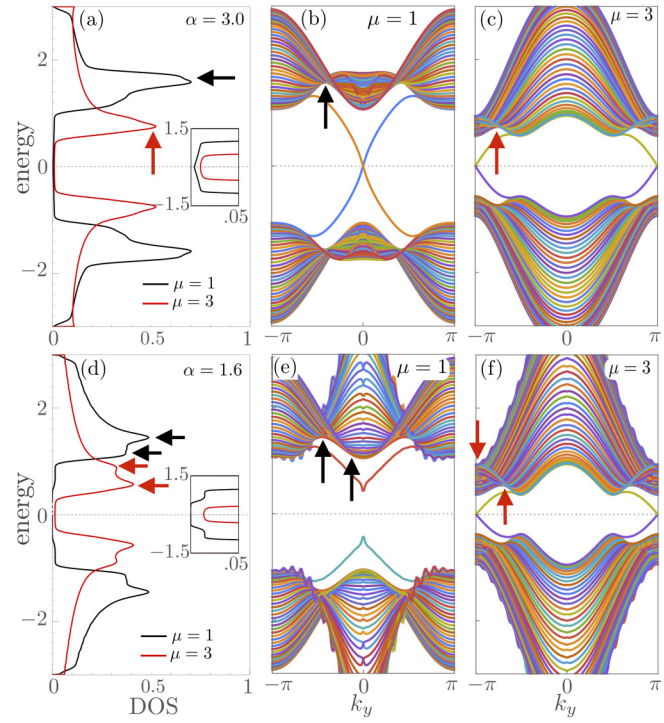

FIG. 2. (a) DOS of a finite squared system for the two phases $\mathcal{M}$ with different chiralities, namely, $\mu = 1$ and $\mu = 3$. Inset: Zoom-in on the in-gap states. (b), (c) Corresponding band spectra for a semi-infinite system, i.e., periodic in the y direction. The many colors represent different energy levels. Arrows indicate the two-peak structure on the DOS and the associated band twist in the band spectrum. (d)–(f) Equivalent results for longer-range couplings; in particular, note that for $\mu = 1$ the system is in phase $\mathcal{D}$.

we note an unusual band twisting (highlighted by the arrows), and (b) there is a significant band overlap as a consequence of this band twisting.

The double-peak structure in the DOS is a measurable consequence of band inversion in topological superconductors. For instance, if the two particle-hole symmetric bands overlapfor small values of Δ, as we increase the superconducting amplitude a gap is opened and a band inversion is formed. Such a band inversion does not happen in the trivial phases. Most notably, in the long-range system with a slow-decaying coupling strength, the band twist (or band inversion) occurs even when the particle-hole bands do not overlap in the limit $\Delta \to 0$. This behavior leads to a higher concentration of densities of states around two areas where the twisting of bands occurs, which in turn generates a double-peak structure in the DOS.

Next we observe that longer-range superconducting couplings are responsible for the enhancement of the peak's structure, in particular, within the massive Dirac phase $\mathcal{D}$. Figures 2(d)–2(f) show the results for smaller values of the superconducting coupling exponent already in phase $\mathcal{D}$, i.e., $\alpha = 1.6$. We clearly see a more pronounced structure of the peaks; more precisely, they split into two peaks, which come along with an enlargement of the band overlap. We further note that the two-peak structure is present in both topological phases and that it is enhanced upon decreasing α, however,

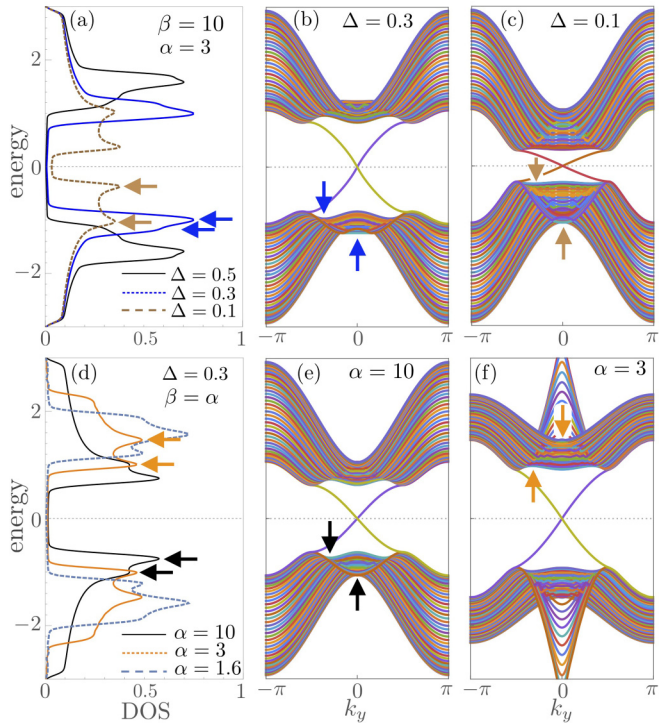

FIG. 3. Here we present results analogous to those in Fig. 2. (a)–(c) Different values of the superconducting coupling strength Δ, in phase $\mathcal{M}$ with $\mu = 1$. (d)–(f) Different values of both the superconducting coupling range (α) and the hopping range (β), for $\mu = 1$ and $\Delta = 0.3$. Note that the change in β is not represented in the phase diagram in Fig. 1(a), but for all the parameter's values shown here the system remains in phase $\mathcal{M}$.

they do not appear in the trivial superconducting phase (not shown in Fig. 2).

The superconducting coupling strength is also responsible for changing the peak structure. In particular, decreasing Δ also makes the peak split into two, as shown in Fig. 3(a). Associated with this, from the semi-infinite system band spectra shown in Figs. 3(b) and 3(c), we again note an enlargement of the band overlap. Indeed, we checked that by lowering Δ (but keeping it finite) the two-peak structure can always be retrieved in all topological phases.

The two-peak structure is not a unique long-range feature. In Figs. 3(d)–3(f) we show the presence of the two peaks even in the fast-decaying limit [$(\beta, \alpha) \gg 1$]. And we have verified that these results match those from a system with short-range hopping. In short, both topological phases present in this work ($\mathcal{M}$ and $\mathcal{D}$) present a double-peak structure in their DOS which is associated with a band twisting, which in turn leads to a band overlap. This association is highlighted by the colored arrows in Figs. 2 and 3. Surprisingly, the DOS double-peak structure only appears within the topological phases. It is always achieved for finite-small values of the superconducting coupling strength and is enhanced by longer-range couplings.

Therefore, within the limitations of the present model these double-peak structures show a nontrivial band topology, due to the effect of band twisting. These results may help us distinguish more easily different topologically trivial and nontrivial phases in experiments.

C. Physical relevance of long-range couplings

As mentioned in Sec. I, p-wave superconductors with long-range couplings naturally appear in different experimental realizations of these materials. A 2D sublattice of magnetic impurities, deposited on the surface of a conventional superconductor, leads to effective long-range pairing and hopping terms with a $1/\sqrt{r}$ decay [43]. In particular, Mn adatoms deposited on top of Pb (001) have been shown to present long-range oscillations of up to 7–8 nm [44], which proves the relevance of long-range interactions in these experiments. We can also consider a different construction, where proximitizing the planar Josephson junction to a 2D electron gas with Rashba spin-orbit coupling and a Zeeman field produces an effective 1D Kitaev chain with long-range pairing and hopping terms [49–51]. The couplings of the effective 1D system can be tuned by varying the superconducting phase difference of the junction ϕ, the in-plane magnetic field B, and the chemical potential μ. The emerging long-range couplings can be intuitively understood as arising from the integration out of closely spaced modes residing along the transverse direction of the 2D electron gas. A similar construction could be used so that the integration of a 3D structure leads to effective long-range couplings in two dimensions. Finally, periodically driving a short-range topological insulator produces interesting effective models of 1D p-wave superconductors where long-range superconductivity arises [48]. Analogously, Floquet driving a planar p-wave superconductor would allow the tuning of effective long-range couplings. In conclusion, we have identified several experimentally relevant situations where the inclusion of long-range coupling terms is needed and where the physics of the topological superconductors described in this paper can be potentially tested.

III. ROBUSTNESS OF THE MASSIVE EDGE STATES AGAINST DISORDER

Here we discuss the effect of static disorder in the presence of massive Dirac states. We first analyze the normalized DOS computed for a finite 2D system with different disorder strengths. The disorder is added to the Hamiltonian as

$$H_{\text{disorder}} = \nu \sum_{\boldsymbol{r}=1}^{N} D_{\boldsymbol{r}} (c_{\boldsymbol{r}}^{\dagger} c_{\boldsymbol{r}} - c_{\boldsymbol{r}} c_{\boldsymbol{r}}^{\dagger}), \tag{2}$$

where ν is the disorder strength and $|D_{\boldsymbol{r}}| \leqslant 1$ is equally distributed over the sites' positions $\boldsymbol{r}$. Other realistic disorder distributions, such as a Gaussian peaked at μ, would be less detrimental to our system and would serve as a less effective test of robustness of the edge states [72].

Figure 4 analyzes the results for a representative point within phase $\mathcal{D}$ (namely, $\mu = 1$, $\alpha = 1.6$, and system size $N = 1681$). Figure 4(a) shows the DOS for different disorder strengths. First, we clearly observe how the DOS peak decreases with this disorder. Second, we show that the bulk gap shrinks more rapidly than the edge gap. In addition, the plateau formed by the massive Dirac edge states (i.e., the finite energies between the bulk gap and the edge gap) remains quantitatively the same even for large values of disorder, i.e., compared to the superconducting gap size, which provides an indication of the robustness of the new massive edge states.

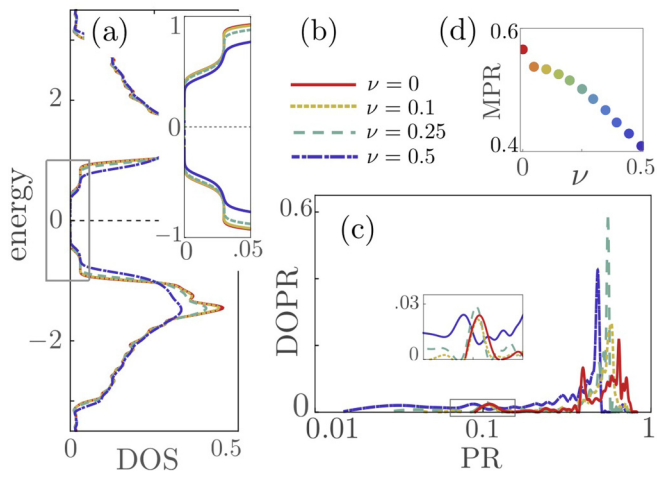

FIG. 4. Behavior of a nonlocal-massive Dirac state (precisely for $\mu = 1$ and $\alpha = 1.6$, for a system size $N = 1681$) in the presence of disorder. (a) DOS. Inset: Zoom-in on the in-gap states. (b) The legend, which holds true for all other panels. (c) The DOPR as a function of the PR for different disorder strengths. Inset: Zoom-in on the peak coming from the edge states. (d) MPR for a range of disorder strengths.

One may also look at the Anderson localization effect from the participation ratio (PR), which gives the degree of localization of each state after one disorder realization, such that

$$\mathrm{PR} \equiv \frac{1}{N}\frac{1}{\sum_{\boldsymbol{r}} \mathcal{P}_n^2(\boldsymbol{r})}. \tag{3}$$

For instance, for a completely delocalized state where all sites are equally likely to be occupied one finds $\mathrm{PR} = 1$, while for a completely localized state where only one site is likely to be occupied one finds $\mathrm{PR} = 1/N$, which goes to 0 at the thermodynamic limit. Moreover, for an edge state perfectly localized at the boundary, i.e., equally distributed along the edge sites of the 2D system, one finds $\mathrm{PR} = 4/\sqrt{N}$.

Figure 4(c) shows a histogram of the participation ratio (which here we call the density of the participation ratio; DOPR) with respect to the energy index (n) for different strengths ν. Note that our results consider 100 disorder realizations, and the results are an average over it. Thus, in this figure one easily notes that the DOPR is concentrated near $\mathrm{PR} = 1$, instead of $\mathrm{PR} \sim 10^{-3}$, for this particular system size, which signals that the bulk states are delocalized. In addition, we note that they continue to be delocalized even for large disorder strengths; i.e., we have considered a maximum disorder of 0.5, while the bulk gap is nearly 1.0 (in units of hopping t) and the edge gap is even smaller. From the edge states we expect a peak near $\mathrm{PR} \approx 0.1$ for this system size, since they are not localized at one point but spread all over the boundary. Thus the inset shows a zoom-in on the DOPR near $\mathrm{PR} = 0.1$. The existing peaks are clear and they shift towards the left with increasing disorder strength, which reflects a trend of the edge states to be more and more localized along the edges.

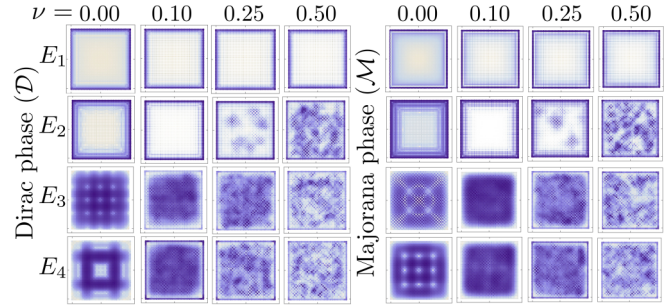

FIG. 5. Spatial distribution of states within phases $\mathcal{D}$ and $\mathcal{M}$. We plotted the probability of occupancy, Φ, associated with the nth energy for a 2D finite-squared system (top view) as described in Figs. 1(d) and 1(e). Each row corresponds to a different representative quantum state with energy E_n, such that E_1 is the lowest finite energy inside the gap; E_2 illustrates the finite energies inside the gap, which goes to the bulk with strong enough disorder. E_3 and E_4 represent two bulk energies. For each of the phases we show what happens to these states after including different values of the disorder strength ν.

The spatial localization over all the states is quantified by the mean participation ratio (MPR), namely,

$$\mathrm{MPR} = \left\langle \frac{1}{2N}\sum_{n=1}^{2N} \mathrm{PR} \right\rangle, \tag{4}$$

where the average $\langle \dots \rangle$ is over disorder realizations. Thus, Fig. 4(d) shows the decreasing of the MPR, roughly from 0.6 to 0.4 with $\nu = 0$ to $\nu = 0.5$, respectively. This shows a trend of the whole system to become more localized, although still orders of magnitude higher than the completely localized value, typically $\mathrm{PR} \approx 6 \times 10^{-4}$ for this system size.

A. Spatial distribution of states

Here we analyze the spatial distribution of states subject to static disorder for both the massive Dirac and the Majorana phases. Each row in Fig. 5 depicts representative states associated with different energy levels. We have considered 100 disorder realizations, and the average was made after sorting the energy spectra and taking equivalent energy levels; for instance, the minimum energy, labeled E_1, was computed as $E_1 = \langle \min(E_n) \rangle$, where $\langle \dots \rangle$ is the average over disorder realizations and $\min(E_n)$ takes the minimum energy value among all the energy levels. The columns in the plot represent different disorder strengths. We note that the energies E_1 to E_4 are not the four lowest energies from the energy spectrum but, rather, energies which correspond to the following behaviors: E_1 is the lowest finite energy inside the gap; E_2 is a finite energy inside the gap and will merge to the bulk after including enough disorder. E_3 and E_4 are two different energies inside the bulk.

Remarkably, the topological robustness of the massive Dirac phase is indeed very similar to the Majorana phase. The topological energy states inside the gap display clear localization along the edges, with a short tail towards the bulk. We have checked that the tail is shortened after including disorder, adding some degree of additional stability to the boundary of the system. The increase in edge localization

through disorder was already noted in the inset in Fig. 4(c), where the peak moves to the left (i.e., towards being more localized). Moreover, Fig. 4(a) shows that the bulk gap is shrinking more rapidly than the edge gap, which means that edge states with higher energies are merging with the bulk. This behavior is illustrated in Fig. 5 by the frames with energy E_2, in which more localized states (like clusters of probability density) are formed inside the bulk. One may note the formation of these clusters for $\nu \geqslant 0.25$. Finally, the bulk states (E_3 and E_4) remain fairly delocalized after incorporating disorder. However, for strong disorder we note the formation of clusters of probability density inside the bulk.

B. Long-range disorder

Some experimental realizations of topological superconductors with long-range couplings may also introduce disorder in the hopping and pairing terms. Therefore, in order to complete the stability analysis of the topological phase, we also introduce disorder perturbations in the hopping and superconducting coupling strengths and compare their relative robustness.

The disorder is introduced by replacing $t \to t + \nu D_{\boldsymbol{r}}(R)$ and $\Delta \to \Delta + \nu D_{\boldsymbol{r}}(R)$ in Eq. (1), with ν setting the disorder strength and $|D_{\boldsymbol{r}}(R)| \leqslant 1$ being a random number equally distributed over the site positions $\boldsymbol{r}$ and long-range parameter R.

In Fig. 6 we depict three situations: (a) the disorder is included only in the hopping strength; (b) the disorder is considered only in the superconducting coupling strength; and (c) the disorder is included in all couplings, the hopping, the pairing, and the chemical potential. In Fig. 6(a) we note that long-range disorder affects the edge states more than short-range disorder, however, the massive Dirac edge modes are clearly robust against weak and moderate disorder; i.e., the in-gap states are present even at $\nu = 0.25$, which is already large compared with the size of the bulk gap. On the other hand, disorder in the superconducting coupling strength is even less harmful. In Fig. 6(b) we see a lowering of the gap's peak with enhancing disorder strength, but the bulk gap is nearly constant. Compared with Fig. 4(a) we see that long-range disorder in the superconducting coupling strength affects the system even less than chemical potential disorder. Finally, in Fig. 6(c) we see that even after including all possible disorder types the largest contribution comes from the hopping, since Figs. 6(a) and 6(c) are very similar. In the second row in Fig. 6 we depict the fate of the massive Dirac modes after including long-range disorder in each case described above. Remarkably, even after including a considerable amount of disorder in all couplings, the edge states are still robust and localized. This is explained by the topological nature of the edge states even with long-range couplings.

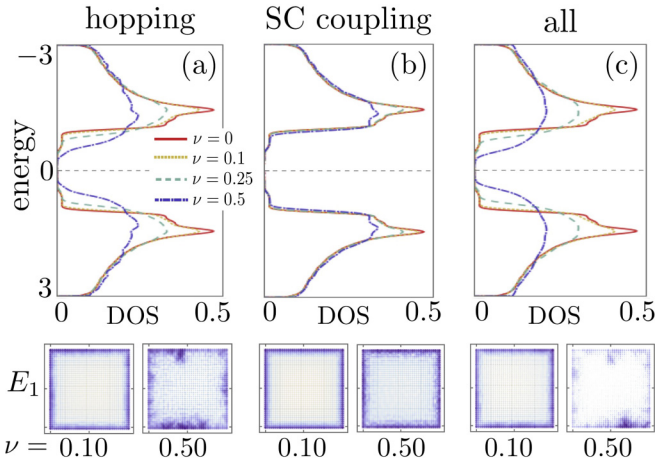

FIG. 6. (a)–(c) DOS in the $\mathcal{D}$ phase and the effect of different types of long-range disorder, where we have used the same parameters as described in Fig. 4. (a) Disorder in the hopping strengths; (b) disorder in the superconducting coupling strengths; (c) both previous cases plus chemical potential disorder. In the second row we plot the probability of occupancy, Φ, associated with the nth energy for a 2D finite-squared system (top view) as described in Figs. 1(d) and 1(e). In each case, we show the lowest finite energy inside the gap, E_1, for two values of disorder strength, namely, $\nu = 0.10$ and $\nu = 0.50$.

IV. DISCUSSION

We have studied the robustness and localization properties of nonlocal-massive Dirac fermions that appear as exotic energy quasiparticles in 2D topological superconductors with long-range interactions. Analyzing the density of states and the energy spectrum, we identify how these topological subgap states at finite energy remain bound to the edge and propagating even for large static disorder. By means of the in-gap states we compute the phase diagram for different chemical potentials and long-range couplings. The propagating massive Dirac fermion is identified from a subgap in the superconducting phase. Looking at the probability of occupancy of the energy spectrum, we can clearly identify the localization properties of massive Dirac fermions along the edges of a 2D square lattice. The robustness of these quasiparticles is tested including chemical potential disorder and long-range disorder. The DOS analysis indicates a strong resistance from the in-gap states to disorder, which is confirmed using a participation ratio analysis of all quantum states in the system. The massive Dirac modes are surprisingly resistant against weak and moderate disorder in the hopping strength, while practically insensitive to disorder in the superconducting coupling strength. Remarkably, the stability of the probability of occupation for the edge states shows that the robustness of the massive Dirac fermions is analogous to that of the Majorana states.

Complementarily, for a semi-infinite-periodic system, we note that a band twisting in the band structure is always accompanied by a double peak in the DOS. We show that this behavior also appears for purely short-range interactions, however, we note that it is an exclusive feature of topological phases and can possibly be used as a probe to identify nontrivial topology. In addition, we show that long-range couplings and low pairing strengths strongly enhance the double-peak structure. This enhancement can be potentially used to experimentally detect topological phases using STM measurements [38].

ACKNOWLEDGMENTS

We thank Pablo San-Jose for providing the MathQ package online, and Tilen Cadez and Liang Fu for useful discussions.

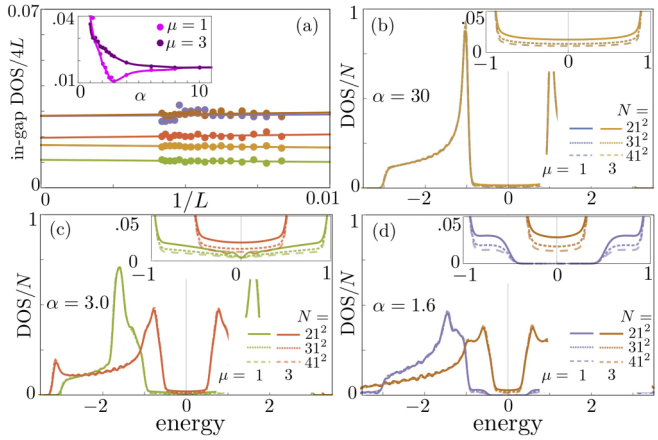

FIG. 7. Finite-size scaling analysis of the in-gap states. (b)–(d) DOS/N for three system sizes and two representative points in the phase diagram, namely, $\mu = 1$ and $\mu = 3$. Each panel is computed for a different α value. Insets: Zoom-ins on the in-gap states. (a) Scaling behavior of the in-gap value DOS/$4L$. The color code represents different μ and α values and follows the legends in (b)–(d); in particular, note that the results corresponding to the parameters used in (b) are degenerated. Inset: Dependence of the in-gap state value on the parameter α, for the two values of μ; solid lines are guides for the eyes.

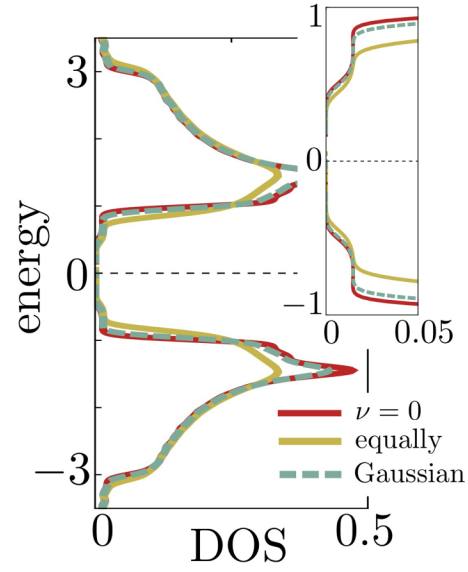

FIG. 8. DOS in the massive Dirac phase (same parameters as in Fig. 4) for different types of static disorder, namely, equally distributed versus Gaussian-distributed disorders in the chemical potential, both computed for $\nu = 0.50$. We also plot the nondisordered case for reference, $\nu = 0$. Inset: Zoom-in on the in-gap states.

This work was supported by Chinese Agencies NSFC (Grant No. 11750110429) and NSAF (Grant No. U1530401), Fundación Ramón Areces, and RCC Harvard.

APPENDIX A: FINITE-SIZE SCALING OF IN-GAP STATES

In Fig. 1(c) in the text, we show the finite DOS inside the superconducting gap. Since the bulk states and the in-gap states are expected to have different finite-size scalings, here we analyze them in detail. In Figs. 7(b)–7(d) we show the DOS for different system sizes and superconducting couplings (controlled by α). In particular, we have used three system sizes, $N = 441$, 961, and 1681, and show results for two representative points in the phase diagram, namely, $\mu = 1$ and $\mu = 3$. The insets show zoom-ins on the in-gap states. We must note that here, as well as in the text, the DOS is normalized by the system size, i.e., DOS $\to$ DOS/N, which explains why they lie on top of each other for different system sizes. Thus now we choose to write this denominator explicitly. On the other hand, the DOS values inside the gap (due to the presence of edges states) are expected to scale with the perimeter ($4\sqrt{N} \equiv 4L$) of the finite system; i.e., rewriting DOS/$N \to$ DOS/$4L$ one finds in-gap states independent of system size, as shown in Fig. 7(a). Finally, we note that the values of the in-gap states are dependent on α. The inset in Fig. 7(a) shows how the exponent α influences the in-gap states. Note that in the case of $\mu = 1$ we have a phase transition, which is accompanied by a change in DOS/$4L$ behavior.

APPENDIX B: GAUSSIAN DISORDER

Here we compare two types of static disorder. Beyond the random-distributed disorder discussed in the text, we also analyze Gaussian-distributed disorder, which is added to the Hamiltonian in Eq. (1) as

$$H^{\mathrm{G}}_{\mathrm{disorder}} = \nu \sum_{\boldsymbol{r}=1}^{N} D^{\mathrm{G}}_{\boldsymbol{r}} (c^{\dagger}_{\boldsymbol{r}} c_{\boldsymbol{r}} - c_{\boldsymbol{r}} c^{\dagger}_{\boldsymbol{r}}), \tag{B1}$$

with ν setting the disorder strength and $D^{G}_{\boldsymbol{r}}$ [$\equiv x(\xi)$ in the following] being a random number weighted by the Gaussian distribution with mean value $\mu = 0$ and standard deviation $\sigma = 0.25$, for each site's position $\boldsymbol{r}$. Namely, from a random number ξ generated in the range $\xi \in (0, 1)$ we can generate a corresponding $x(\xi) \in (-\infty, +\infty)$ weighted by a Gaussian distribution through the equation $x(\xi) = \mu + \sigma\sqrt{2}\mathrm{err}^{-1}(2\xi - 1)$, where err^{-1} is the inverse of the error function. The latter expression is obtained from the inverse of the cumulant of the Gaussian function. In principle, the cumulant of any normalized distribution can be associated with the random variable ξ; in particular, for the Gaussian distribution we have $\xi = \int_{-\infty}^{x} \mathrm{e}^{-(x'-\mu)^2/(2\sigma^2)}/(\sigma\sqrt{2\pi})dx'$.

As shown in Fig. 8, Gaussian disorder is less harmful to the system than equally spaced disorder, which is the case considered throughout the paper as a benchmark for robustness.

[1] M. Z. Hasan and C. L. Kane, Rev. Mod. Phys. **82**, 3045 (2010).
[2] X.-L. Qi and S.-C. Zhang, Rev. Mod. Phys. **83**, 1057 (2011).
[3] N. Read and D. Green, Phys. Rev. B **61**, 10267 (2000).
[4] B. A. Bernevig and T. L. Hughes, *Topological Insulators and Topological Superconductors* (Princeton University Press, Princeton, NJ, 2013).

[5] C. Nayak, S. H. Simon, A. Stern, M. Freedman, and S. Das Sarma, Rev. Mod. Phys. **80**, 1083 (2008).
[6] B. M. Terhal, Rev. Mod. Phys. **87**, 307 (2015).
[7] J. Alicea, Y. Oreg, G. Refael, F. von Oppen, and M. P. A. Fisher, Nat. Phys. **7**, 412 (2011).
[8] C. V. Kraus, P. Zoller, and M. A. Baranov, Phys. Rev. Lett. **111**, 203001 (2013).
[9] L. Mazza, M. Rizzi, M. D. Lukin, and J. I. Cirac, Phys. Rev. B **88**, 205142 (2013).
[10] A. Y. Kitaev, Phys.-Usp. **44**, 131 (2001).
[11] L. Fu and C. L. Kane, Phys. Rev. Lett. **100**, 096407 (2008).
[12] J.-P. Xu, M.-X. Wang, Z. L. Liu, J.-F. Ge, X. Yang, C. Liu, Z. A. Xu, D. Guan, C. L. Gao, D. Qian, Y. Liu, Q.-H. Wang, F.-C. Zhang, Q.-K. Xue, and J.-F. Jia, Phys. Rev. Lett. **114**, 017001 (2015).
[13] H.-H. Sun, K.-W. Zhang, L.-H. Hu, C. Li, G.-Y. Wang, H.-Y. Ma, Z.-A. Xu, C.-L. Gao, D.-D. Guan, Y.-Y. Li, C. Liu, D. Qian, Y. Zhou, L. Fu, S.-C. Li, F.-C. Zhang, and J.-F. Jia, Phys. Rev. Lett. **116**, 257003 (2016).
[14] J. D. Sau, R. M. Lutchyn, S. Tewari, and S. Das Sarma, Phys. Rev. Lett. **104**, 040502 (2010).
[15] J. Alicea, Phys. Rev. B **81**, 125318 (2010).
[16] J. D. Sau, S. Tewari, R. M. Lutchyn, T. D. Stanescu, and S. Das Sarma, Phys. Rev. B **82**, 214509 (2010).
[17] R. M. Lutchyn, J. D. Sau, and S. Das Sarma, Phys. Rev. Lett. **105**, 077001 (2010).
[18] Y. Oreg, G. Refael, and F. von Oppen, Phys. Rev. Lett. **105**, 177002 (2010).
[19] V. Mourik, K. Zuo, S. M. Frolov, S. R. Plissard, E. P. A. M. Bakkers, and L. P. Kouwenhoven, Science **336**, 1003 (2012).
[20] M. T. Deng, C. L. Yu, G. Y. Huang, M. Larsson, P. Caroff, and H. Q. Xu, Nano Lett. **12**, 6414 (2012).
[21] A. Das, Y. Ronen, Y. Most, Y. Oreg, M. Heiblum, and H. Shtrikman, Nat. Phys. **8**, 887 (2012).
[22] M.-X. Wang, C. Liu, J.-P. Xu, F. Yang, L. Miao, M.-Y. Yao, C. L. Gao, C. Shen, X. Ma, X. Chen, Z.-A. Xu, Y. Liu, S.-C. Zhang, D. Qian, J.-F. Jia, and Q.-K. Xue, Science **336**, 52 (2012).
[23] L. P. Rokhinson, X. Liu, and J. K. Furdyna, Nat. Phys. **8**, 795 (2012).
[24] H. O. H. Churchill, V. Fatemi, K. Grove-Rasmussen, M. T. Deng, P. Caroff, H. Q. Xu, and C. M. Marcus, Phys. Rev. B **87**, 241401(R) (2013).
[25] Q. L. He, H. Liu, M. He, Y. H. Lai, H. He, G. Wang, K. T. Law, R. Lortz, J. Wang, and I. K. Sou, Nat. Commun. **5**, 4247 (2014).
[26] S. M. Albrecht, A. P. Higginbotham, M. Madsen, F. Kuemmeth, T. S. Jespersen, J. Nygård, P. Krogstrup, and C. M. Marcus, Nature **531**, 206 (2016).
[27] M. T. Deng, S. Vaitiekenas, E. B. Hansen, J. Danon, M. Leijnse, K. Flensberg, J. Nygård, P. Krogstrup, and C. M. Marcus, Science **354**, 1557 (2016).
[28] Q. L. He, L. Pan, A. L. Stern, E. C. Burks, X. Che, G. Yin, J. Wang, B. Lian, Q. Zhou, E. S. Choi, K. Murata, X. Kou, Z. Chen, T. Nie, Q. Shao, Y. Fan, S.-C. Zhang, K. Liu, J. Xia, and K. L. Wang, Science **357**, 294 (2017).
[29] R. M. Lutchyn, E. P. A. M. Bakkers, L. P. Kouwenhoven, P. Krogstrup, C. M. Marcus, and Y. Oreg, Nat. Rev. Mater. **3**, 52 (2018).
[30] F. Pientka, L. I. Glazman, and F. von Oppen, Phys. Rev. B **88**, 155420 (2013).
[31] B. Braunecker and P. Simon, Phys. Rev. Lett. **111**, 147202 (2013).
[32] S. Nadj-Perge, I. K. Drozdov, B. A. Bernevig, and A. Yazdani, Phys. Rev. B **88**, 020407(R) (2013).
[33] J. Klinovaja, P. Stano, A. Yazdani, and D. Loss, Phys. Rev. Lett. **111**, 186805 (2013).
[34] F. Pientka, L. I. Glazman, and F. von Oppen, Phys. Rev. B **89**, 180505(R) (2014).
[35] T. Neupert, A. Yazdani, and B. A. Bernevig, Phys. Rev. B **93**, 094508 (2016).
[36] V. Kaladzhyan, C. Bena, and P. Simon, J. Phys.: Condens. Matter **28**, 485701 (2016).
[37] V. Kaladzhyan, J. Röntynen, P. Simon, and T. Ojanen, Phys. Rev. B **94**, 060505(R) (2016).
[38] S. Nadj-Perge, I. K. Drozdov, J. Li, H. Chen, S. Jeon, J. Seo, A. H. MacDonald, B. A. Bernevig, and A. Yazdani, Science **346**, 602 (2014).
[39] M. Ruby, F. Pientka, Y. Peng, F. von Oppen, B. W. Heinrich, and K. J. Franke, Phys. Rev. Lett. **115**, 197204 (2015).
[40] R. Pawlak, M. Kisiel, J. Klinovaja, T. Meier, S. Kawai, T. Glatzel, D. Loss, and E. Meyer, Npj Quantum Info. **2**, 16035 (2016).
[41] M. Ruby, B. W. Heinrich, Y. Peng, F. von Oppen, and K. J. Franke, Nano Lett. **17**, 4473 (2017).
[42] G. C. Ménard, S. Guissart, C. Brun, S. Pons, V. S. Stolyarov, F. Debontridder, M. V. Leclerc, E. Janod, L. Cario, D. Roditchev, P. Simon, and T. Cren, Nat. Phys. **11**, 1013 (2015).
[43] G. C. Ménard, S. Guissart, C. Brun, R. T. Leriche, M. Trif, F. Debontridder, D. Demaille, D. Roditchev, P. Simon, and T. Cren, Nat. Commun. **8**, 2040 (2017).
[44] B. W. Heinrich, J. I. Pascual, and K. J. Franke, Prog. Surf. Sci. **93**, 1 (2018).
[45] J. Röntynen and T. Ojanen, Phys. Rev. Lett. **114**, 236803 (2015).
[46] J. Li, T. Neupert, Z. Wang, A. H. MacDonald, A. Yazdani, and B. A. Bernevig, Nat. Commun. **7**, 12297 (2016).
[47] D.-J. Choi, C. Rubio-Verdú, J. de Bruijckere, M. M. Ugeda, N. Lorente, and J. I. Pascual, Nat. Commun. **8**, 15175 (2017).
[48] M. Benito, A. Gómez-León, V. M. Bastidas, T. Brandes, and G. Platero, Phys. Rev. B **90**, 205127 (2014).
[49] F. Pientka, A. Keselman, E. Berg, A. Yacoby, A. Stern, and B. I. Halperin, Phys. Rev. X **7**, 021032 (2017).
[50] D. T. Liu, J. Shabani, and A. Mitra, Phys. Rev. B **97**, 235114 (2018).
[51] A. Fornieri, A. M. Whiticar, F. Setiawan, E. Portolés, A. C. C. Drachmann, A. Keselman, S. Gronin, C. Thomas, T. Wang, R. Kallaher, G. C. Gardner, E. Berg, M. J. Manfra, A. Stern, C. M. Marcus, and F. Nichele, Nature **569**, 89 (2019).
[52] Y. Niu, S. B. Chung, C.-H. Hsu, I. Mandal, S. Raghu, and S. Chakravarty, Phys. Rev. B **85**, 035110 (2012).
[53] W. DeGottardi, M. Thakurathi, S. Vishveshwara, and D. Sen, Phys. Rev. B **88**, 165111 (2013).
[54] D. Vodola, L. Lepori, E. Ercolessi, A. V. Gorshkov, and G. Pupillo, Phys. Rev. Lett. **113**, 156402 (2014).
[55] A. González-Tudela, C. L. Hung, D. E. Chang, J. I. Cirac, and H. J. Kimble, Nat. Photon. **9**, 320 (2015).
[56] D. Vodola, L. Lepori, E. Ercolessi, and G. Pupillo, New J. Phys. **18**, 015001 (2015).
[57] O. Viyuela, D. Vodola, G. Pupillo, and M. A. Martin-Delgado, Phys. Rev. B **94**, 125121 (2016).

[58] Z.-X. Gong, M. F. Maghrebi, A. Hu, M. L. Wall, M. Foss-Feig, and A. V. Gorshkov, Phys. Rev. B **93**, 041102(R) (2016).
[59] Z.-X. Gong, M. F. Maghrebi, A. Hu, M. Foss-Feig, P. Richerme, C. Monroe, and A. V. Gorshkov, Phys. Rev. B **93**, 205115 (2016).
[60] K. Patrick, T. Neupert, and J. K. Pachos, Phys. Rev. Lett. **118**, 267002 (2017).
[61] L. Lepori and L. Dell'Anna, New J. Phys. **19**, 103030 (2017).
[62] A. Alecce and L. Dell'Anna, Phys. Rev. B **95**, 195160 (2017).
[63] L. Lepori, A. Trombettoni, and D. Vodola, J. Stat. Mech.: Theor. Exp. (2017) 033102.
[64] A. Dutta and A. Dutta, Phys. Rev. B **96**, 125113 (2017).
[65] P. Cats, A. Quelle, O. Viyuela, M. A. Martin-Delgado, and C. Morais Smith, Phys. Rev. B **97**, 121106(R) (2018).
[66] D. Giuliano, S. Paganelli, and L. Lepori, Phys. Rev. B **97**, 155113 (2018).
[67] O. Viyuela, L. Fu, and M. A. Martin-Delgado, Phys. Rev. Lett. **120**, 017001 (2018).
[68] L. Lepori, D. Giuliano, and S. Paganelli, Phys. Rev. B **97**, 041109(R) (2018).
[69] See Appendix A for a finite-size scaling analysis of the in-gap states and their dependence on the decay exponent α.
[70] A. P. Schnyder, S. Ryu, A. Furusaki, and A. W. W. Ludwig, Phys. Rev. B **78**, 195125 (2008).
[71] For instance, in k space the Hamiltonian assumes the form $H = \mathrm{even(k)}\sigma_z + \mathrm{odd(k)}(\sigma_x + \mathrm{i}\sigma_y)$, where σ acts on the Nambu basis. Thus, the particle-hole operator is $\mathcal{P} \equiv \sigma_x K$, which satisfies the relation $H_k = -\mathcal{P}H_{-k}\mathcal{P}$ or the relation $H = -\mathcal{P}H^T\mathcal{P}$ in real space. It also has inversion symmetry, whose operator is $\mathcal{I} \equiv \sigma_z$ and respects the relation $H_k = \mathcal{I}H_{-k}\mathcal{I}$ or the relation $H_{\boldsymbol{R}} = \mathcal{I}H_{-\boldsymbol{R}}\mathcal{I}$ in real space.
[72] See Appendix B, where we compare different types of disorder.